JOURNAL OF MODERN OPTICS, 1990, VOL. 37, NO. 5, 965–975

Numerical solution of the fourth-moment equation for a point source

D. E. REEVE†, S. R. LEONARD

Marconi Maritime Applied Research Laboratory, Unit 32-35, Science Park, Milton Road, Cambridge CB4 4FX, England

and M. SPIVACK

Department of Applied Mathematics and Theoretical Physics, University of Cambridge, Silver Street, Cambridge CB3 9EW, England

(*Received 27 July 1989 and accepted 29 September 1989*)

Abstract. This paper presents an accurate numerical solution of the fourth-moment equation for a point source. This moment describes the intensity fluctuations arising from wave propagation in random media. The problem has remained intractible due to the nature of the solution and its rapid evolution with range. An adaptive grid method has been developed to deal with these difficulties, and its application to this equation provides a reliable and efficient way of obtaining solutions for a wide range of scattering strengths.

1. Introduction

The study of intensity fluctuations which arise from wave propagation in two-dimensional random media has received considerable attention in recent years. For an incident plane wave, accurate numerical solutions [1, 2] have confirmed and extended the analytical results of [3, 4]. The more important problem of propagation from a point source in a two-dimensional plane, however, has proved far more intractable. The difficulty in numerical approaches lies in the rapid variation of the fourth moment with propagation, and the large ratio between its characteristic scale sizes; this is due mainly to the range dependence of the scattering and diffraction operators. Although related theoretical results have appeared previously [4], they are restricted to the case of a finite beamed source. Numerical results for a beamed source [5] have been presented only for very small values of scattering strength Γ.

The purpose of this paper is to present an accurate, efficient numerical solution of the fourth-moment equation for a point source, valid for a wide range of scattering strengths. The difficulties are overcome by means of an adaptive grid technique, developed for this purpose and described in [2]. The accuracy of the results is confirmed by comparison with the operator splitting method [1], which is cumbersome and inefficient when applied to a point source.

In section 2 a description of the fourth-moment equation for a point source is given, with the mathematical background. The numerical techniques used in solving the fourth-moment equations are described in section 3. The results are presented in section 4. Both the scintillation index, and power spectra of intensity fluctuations, are calculated as functions of range and Γ.

† Present address: Sir William Halcrow & Partners, Burderop Park, Swindon, Wiltshire, SN4 0QD, England.

0950-0340/90 $3·00

2. The fourth-moment equation

The derivation of the fourth-moment equation for a point source has been given elsewhere [6] and will only be sketched here.

Let the monochromatic source, with frequency ω, be situated at the origin of a cylindrical set of coordinates, (r, θ). The wave field, p, may be written as

$$p(r,\theta) = E(r,\theta)\exp[-\mathrm{i}(kr-\omega t)]r^{-1/2}, \tag{1}$$

where k is the wavenumber. Here, the exponential represents harmonic variation and the factor $r^{-1/2}$ is due to cylindrical spreading, so that E is the slowly-varying stochastic component of the complex wave field. Propagation is currently restricted to the two-dimensional range-declination plane. Let

$$n = \langle n\rangle + \mu n_1(r,\theta) \tag{2}$$

be the refractive index of the medium, where angled brackets denote an ensemble average. The stochastically varying part of the refractive index is written as μn_1, and has variance μ, where n_1 is a stationary Gaussian random variable with zero mean and unit variance. The mean $\langle n\rangle$ will be assumed to be constant. Let ρ denote the autocorrelation function of n_1.

$$\rho(r,r',\theta,\theta') = \langle n_1(r,\theta)n_1(r',\theta')\rangle. \tag{3}$$

It will be assumed that ρ depends only on spatial separation, and has a scale-size L, which is much greater than a wavelength $2\pi/k$. Thus E obeys the usual paraxial wave equation,

$$E_r{}^2 = -(\mathrm{i}/2kr^2)E_{\theta\theta} - (\mathrm{i}k\mu n_1/2)E, \tag{4}$$

satisfying the initial condition $E(0,\theta)\equiv 1$. The fourth moment for E is the averaged quantity

$$m = \langle E(r_1,\theta_1)E^*(r_2,\theta_2)E(r_3,\theta^3)E^*(r_4,\theta_4)\rangle, \tag{5}$$

which yields the autocorrelation and spectrum of intensity fluctuations.

Now, put $R' = (r+r')/2$ and $S = r-r'$, and let

$$\rho_{ij} = \int \rho(r,r',\theta_i,\theta_j)\,\mathrm{d}S. \tag{6}$$

Put $\rho_0 = \rho_{ii}$. It follows from the assumptions above that ρ_0 and ρ_{ij} are well defined, and that (for small angular separations) ρ_{ij} is approximately a function of $R'(\theta_i-\theta_j)$. Let f be the normalised autocorrelation function $f(R'(\theta_i-\theta_j)) = \rho_{ij}/\rho_0$. Then, for example, in the case of a Gaussian medium,

$$f(\phi) = \exp(-\phi^2/L^2). \tag{7}$$

It may now be shown that the propagation of the fourth moment, m, is governed by the partial differential equation,

$$m_{R'} = -(\mathrm{i}/2kR'^2)(\nabla_1^2 - \nabla_2^2 + \nabla_3^2 - \nabla_4^2)m - k^2\mu^2 hm,$$

where

$$\nabla_j^2 \equiv \partial^2/\partial\theta_j^2,$$

$$h = 2\rho_0 + \rho_{13} + \rho_{24} - \rho_{12} - \rho_{23} - \rho_{14} - \rho_{34}. \tag{8}$$

Introducing the following change of variables,

$$\xi=(\theta_1-\theta_2-\theta_3+\theta_4)kL/2,$$
$$\eta=(\theta_1+\theta_2-\theta_3-\theta_4)kL/2,$$
$$Z=R'/kL^2,$$

allows equation (8) to be written in transformed coordinates as

$$m_Z=-\mathrm{i}Z^{-2}m_{\xi\eta}-2\Gamma[1-g(Z\xi,Z\eta)]m, \tag{9}$$

where $g(\phi,\psi)=f(\phi)+f(\psi)-[f(\phi+\psi)+f(\phi-\psi)]$, and $\Gamma=k^3\mu^2L^2\rho_0$ is the scattering strength parameter. This is the form of the equation which will be used in finding the numerical solutions.

Quantities of interest such as the variance, autocorrelation function and power spectrum of the intensity fluctuations may be obtained from the fourth moment. Writing I_i as $E(r,\theta_i)^*(r,\theta_i)$, the autocorrelation function of intensity fluctuations, ρ_I, can be written in terms of the fourth moment as:

$$\rho_I=\langle I_1I_2\rangle-1=m(\xi,0,Z). \tag{10}$$

The power spectrum of the intensity fluctuations, $\Phi(\nu)$, is calculated from the Fourier transform of the autocorrelation function,

$$\Phi(\nu)=(1/2\pi)\int\rho_I(\xi)\exp(-\mathrm{i}\nu\xi)\,\mathrm{d}\xi, \tag{11}$$

while the scintillation index, the variance of the intensity fluctuations, may be calculated by integrating the power spectrum over all wavenumbers,

$$\sigma_I^2=\int\Phi(\nu)\,\mathrm{d}\nu. \tag{12}$$

Both the integrals in equations (11) and (12) are performed over the interval $(-\infty, \infty)$.

2.1. *Symmetries*

The function $m(\xi,\eta,Z)$ satisfies the following symmetries which will be used in section 3:

$$m(\xi,\eta,Z)=m(\eta,\xi,Z)=m(-\xi,-\eta,Z), \tag{13}$$
$$m(\xi,\eta,Z)=m^*(\xi,-\eta,Z)=m^*(-\xi,\eta,Z). \tag{14}$$

3. The numerical solution

Equation (9) was solved using an adaptive grid algorithm, and compared with results obtained from an operator splitting method (OSM). The OSM has been used successfully to solve the fourth-moment equation for a plane wave for both single [1] and multiple frequencies [7]. It can be tailored to solve the fourth-moment equation for a point source but has difficulty in resolving the widely separated scales. The main method that has been developed uses an adaptive grid algorithm. This has been demonstrated to give accurate and efficient solutions to the fourth-moment equation [2]. Brief descriptions of the adaptive grid and operator splitting methods, as applied to the point source equation, (9), are presented below.

3.1. *The adaptive grid algorithm*

Equation (9) was discretised by replacing the variables ξ and η with the grid points ξ_i and η_j, with $i,j=0,1,\ldots,N$. In general, adaptive grid methods [8, 9] allow the grid points to vary with range and this can lead to high accuracy and low storage requirements. Here, the grid points are constrained to move on lines parallel to the $\xi-$ and $\eta-$ axes. Such a method has already been developed to solve the fourth-moment equation for a plane wave [2]. The adaptive grid algorithm (AGA) which is used here is an extension of that method. Some modification is required to cope with the increased concentration of the fourth moment along the axes for the case of a point source. The parameter α, in equation (12) of [2], which is a lower bound on the ratio of the smallest to largest grid spacings, is now specified as a function of range. Near the source it was found that for small values of α, extremely small range steps had to be taken in order to maintain the chosen error tolerance. With larger values of α the step size could be increased, without any noticeable change in the solution. However, small values of α were required to resolve the fine detail at larger ranges, and so α was allowed to decrease exponentially with range.

As found in the plane wave case, the reflective symmetry (13) allows the grid spacing along lines parallel to the ξ and η axes to be the same. The symmetry (13) and conjugate symmetry (14) allow us to impose periodic boundary conditions, period $2H$. Therefore, equation (9) need only be solved over a triangular region given by $0\leqslant\eta\leqslant\xi\leqslant H$, for the solution to be known throughout the whole domain. Here H is the maximum value of ξ or η used in the discretisation.

Following the approach of [2], equation (9) is solved computationally in the following form,

$$u_t=m_\xi\xi_t+m_\eta\eta_t-\mathrm{i}Z^{-2}m_{\xi\eta}-2\Gamma[1-g(Z\xi,Z\eta)]m, \tag{15}$$

which is (9) with $m(\xi,\eta,Z)=u(x,y,t)$, and the change of variables $\xi,\eta,Z\rightarrow x,y,t$, where x, y and t are independent variables with respect to which the grid points are fixed.

3.2. *The operator splitting method*

The operator splitting method (OSM) for a plane wave is described in [1]. Its application to a point source is similar and can be summarised briefly as follows. The differences which arise are due mainly to the range dependence of the operators in equation (9).

The formal solution of equation (9) over a range ΔZ may be written approximately as

$$m(Z+\Delta Z)\cong\exp\left[\int_Z^{Z+\Delta Z}(A+B)\,\mathrm{d}Z\right]m(Z), \tag{16}$$

where

$$A=-\mathrm{i}Z^{-2}\partial^2/\partial\xi\partial\eta,$$

$$B=-2\Gamma[1-g(Z\xi,Z\eta)].$$

The equivalent plane wave solution is exact because the corresponding operator $(A+B)$ commutes with its integral, (see [10]). Equation (16) can be further

approximated by

$$m(Z+\Delta Z)\cong\exp\left[\int_Z^{Z+\Delta Z} A\,\mathrm{d}Z\right]\exp\left[\int_Z^{Z+\Delta Z} B\,\mathrm{d}Z\right]m(Z), \tag{17}$$

or, to higher order,

$$m(Z+\Delta Z)\cong\exp\left[\int_Z^{Z+\Delta Z} A/2\,\mathrm{d}Z\right]\exp\left[\int_Z^{Z+\Delta Z} B\,\mathrm{d}Z\right]\exp\left[\int_Z^{Z+\Delta Z} A/2\,\mathrm{d}Z\right]m(Z). \tag{18}$$

The advantage of this splitting is that each exponential in (17) and (18) may be solved accurately. The operator $\exp(\int B\,\mathrm{d}Z)$ is simply a function which, in most cases of interest, will be known exactly. The exponential $\exp(\int A\,\mathrm{d}Z)$ may be solved, as in [1], by use of the fast Fourier transform, F:

$$\exp\left(\int_Z^{Z+\Delta Z} A\,\mathrm{d}Z\right)m(\xi,\eta,Z)=F^{-1}\left\{\exp\left[-\frac{\mathrm{i}\nu_1\nu_2\,\Delta Z}{Z(Z+\Delta Z)}\right]F(m)\right\}, \tag{19}$$

where ν_1 and ν_2 are the transform variables corresponding to ξ and η. Thus both $\exp(\int B\,\mathrm{d}Z)$ and $\exp(\int A\,\mathrm{d}Z)$ are range-dependent. These solutions are applied alternately, and the procedure carried out repeatedly to any range.

The OSM provides a powerful technique when a fixed, uniform grid may be used [1]. For the point source, however, it becomes prohibitive for two reasons. Firstly, the solution has features with both large and small scale sizes, whose ratio increases with range. Secondly, the overall domain of variation in the (ξ,η) plane contracts rapidly with range. To capture this behaviour adequately a fixed grid method would require around 10^7 grid-points in total. In order to overcome this, a nested sequence of regular grids was used, covering successively smaller regions of the (ξ,η) plane. As it became necessary the solution was transferred onto a smaller grid using interpolation, and continued until another change of grid was required. This laborious and inefficient procedure nevertheless gives accurate results, especially at small ranges, for values of Γ up to 50.

4. Results

The difficulties encountered in numerically integrating equation (9) are most clearly explained with figures of the fourth-moment function. All integrations were performed on a half period of $H=2500$ with $N=50$, so the region of solution is $\xi,\eta\in[0,2500]$. Figures 1 and 2 show the real and imaginary components of the fourth moment for $\Gamma=25$ at ranges of $Z=0{\cdot}625$ and $1{\cdot}25$ respectively. The part of the domain shown is $\xi,\eta\in[0,9{\cdot}5]$. This corresponds to 35 and 42 grid points along each axis in figures 1 and 2 respectively. The hardest characteristic of the fourth moment for any numerical method to capture accurately is its evolution at two widely separated length scales. These are best exemplified by the sharp 'ridge' pattern along the axes and the peak at the origin in the real part of the fourth moment, and the long thin spurs in the imaginary part which run parallel to, but offset from, the axes. With fixed, equispaced grid methods, a grid spacing sufficiently small to resolve the small scale features will lead to gross inefficiency in describing the large scale features. The ability of the adaptive grid algorithm to increase and decrease the density of points, in regions of rapid and gradual variation of the fourth moment respectively, is clear from these figures.

Figures 1 and 2 illustrate the manner in which the real and imaginary components evolve as range increases. In the real part, the peak at the origin and the ridges along the axes become narrower. The imaginary part changes in a different way. Although its maximum values are of a lower order of magnitude, the imaginary component has a profound effect on the propagation of $m(\xi, \eta, Z)$. In particular, the changes in the long spurs running parallel to the axes, not immediately apparent in figures 1 and 2, are important.

Figure 3 compares results using the AGA, (full line), with those using the OSM, (broken line). The scintillation index is plotted as a function of range for $\Gamma = 50$. The curves agree extremely well up to $Z \approx 0{\cdot}5$. Beyond this point it becomes increasingly difficult for the OSM to fully capture the behaviour of the fourth moment. This is because it can no longer resolve the fine detail in the real part and the large scale variation in the imaginary part simultaneously.

The dependence of the position and height of the peak in the scintillation index on the scattering parameter Γ is shown clearly in figure 4. The full, dotted and dashed curves correspond to $\Gamma = 50$, 25 and 12·5 respectively. The veracity of the

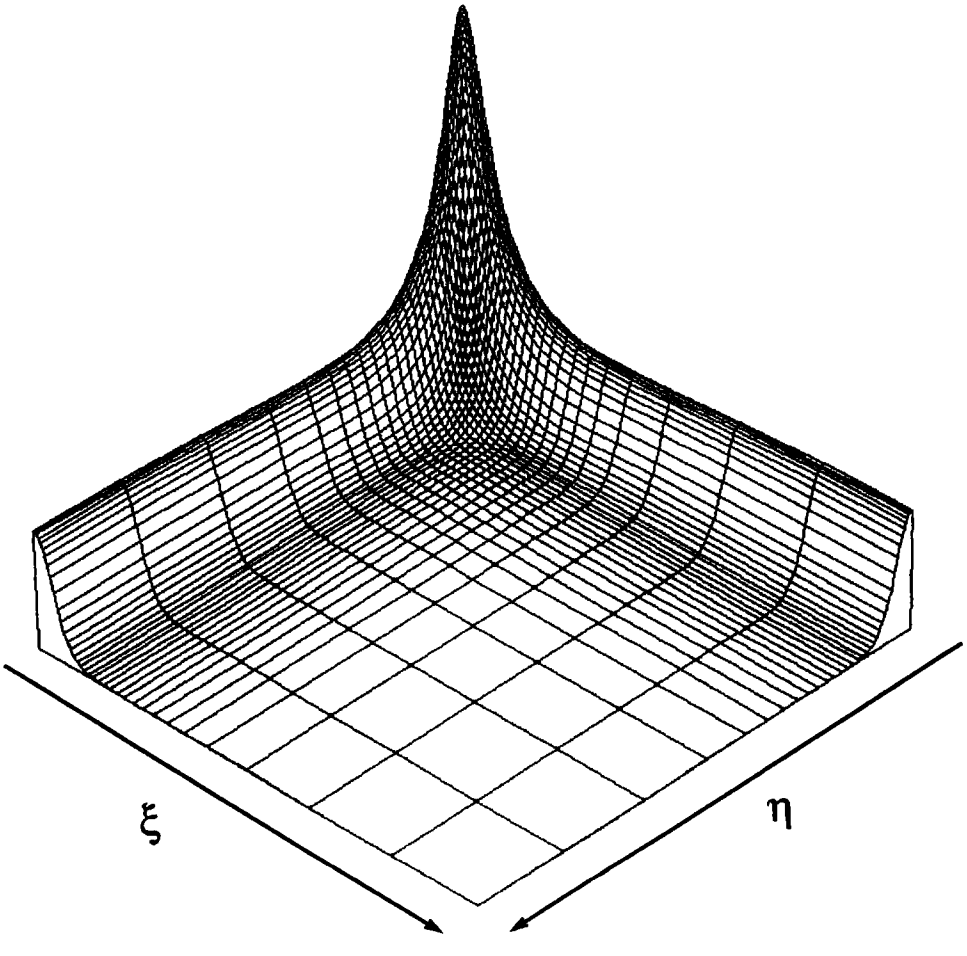

(*a*)

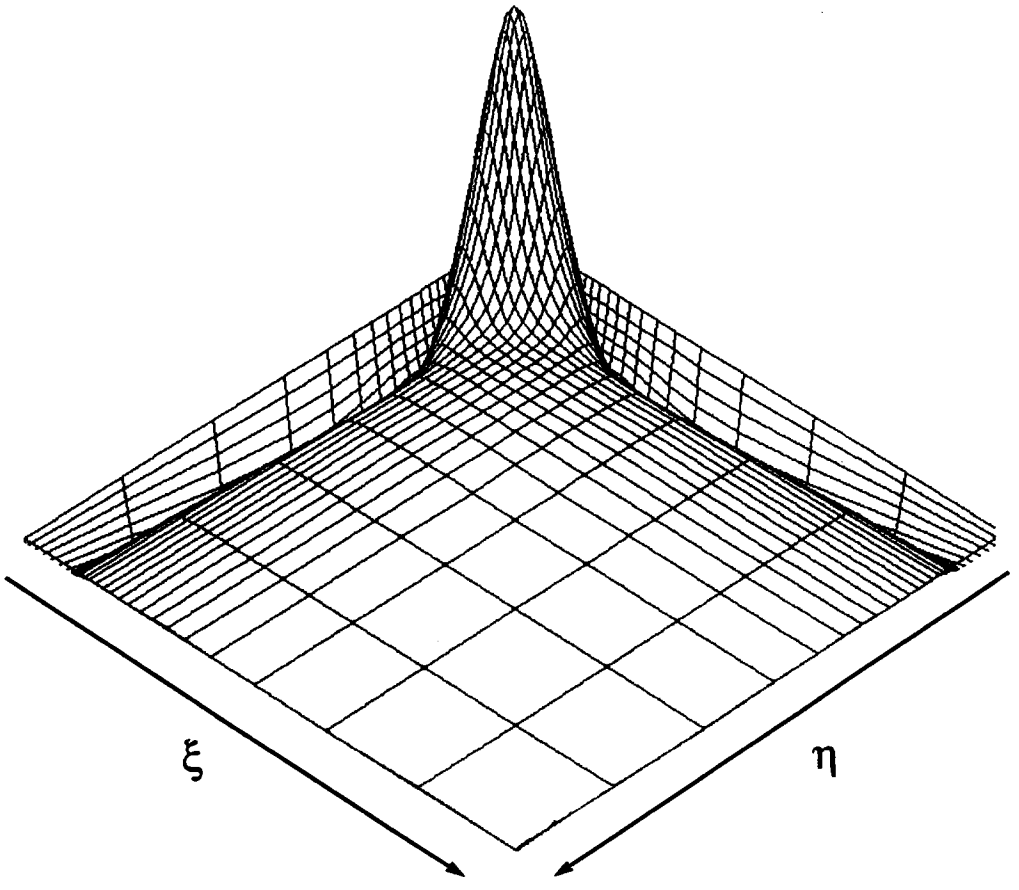

(*b*)

Figure 1 (*a*). The real part of the fourth moment at $Z=0{\cdot}625$ with $\Gamma=25$. The coordinates ξ and η both range from 0 to $\sim 9{\cdot}5$. The vertical scale runs from 0 to 2·95. (*b*). The imaginary part of the fourth moment at $Z=0{\cdot}625$ with $\Gamma=25$. The coordinates ξ and η both range from 0 to $\sim 9{\cdot}5$. The vertical scale runs from $-4{\cdot}25\times10^{-2}$ to $7{\cdot}5\times10^{-2}$.

numerical solutions may be tested by assessing their stability with respect to changes in parameters such as H and N. For the values given above for H and N, the solutions had converged, and further increases in these parameters had negligible effect.

Comparing the scintillation index curves in figure 4 to those obtained for a plane wave reveals several interesting differences. Firstly, the rise in the scintillation index is initially much slower in the point source case. As a rule of thumb, for a given value of Γ, the maximum in the scintillation index for a point source occurs at about four times the range that it does for a plane wave. Secondly, for each value of Γ, this maximum is greater in the case of a point source. After a period of relatively rapid increase in scintillation index the curves begin to level off, at a range Z_{f_1}, say.

However, at this stage the scintillation index is still rising and the peak is not reached until a range $Z_{f_2} \approx 2Z_{f_1}$.

In addition to considering the scintillation index, it is useful to examine the power spectrum, equation (11). This provides information on the scale-size content of the intensity fluctuations. Figure 5 shows power spectra $\Gamma = 50$ at ranges of $Z = 0{\cdot}5\,Z_{f_2}$, Z_{f_2} and $1{\cdot}5\,Z_{f_2}$ respectively. Again, comparison between the power spectra for the point source in figure 5 and those obtained for a plane wave, reveals significant differences. Firstly, the overall power levels of the spectra are several times larger for the point source. Secondly, the spectra for the plane wave given in [1] show only a small amount of broadening at high wavenumbers as Z increases. This is in marked contrast to the spectra shown in figure 5, where considerable broadening of the spectra is apparent at high wavenumbers as Z increases. Finally, there is significant power at low wavenumbers. These power spectra illustrate the extremely wide range of scales present in the intensity fluctuations for the point source problem.

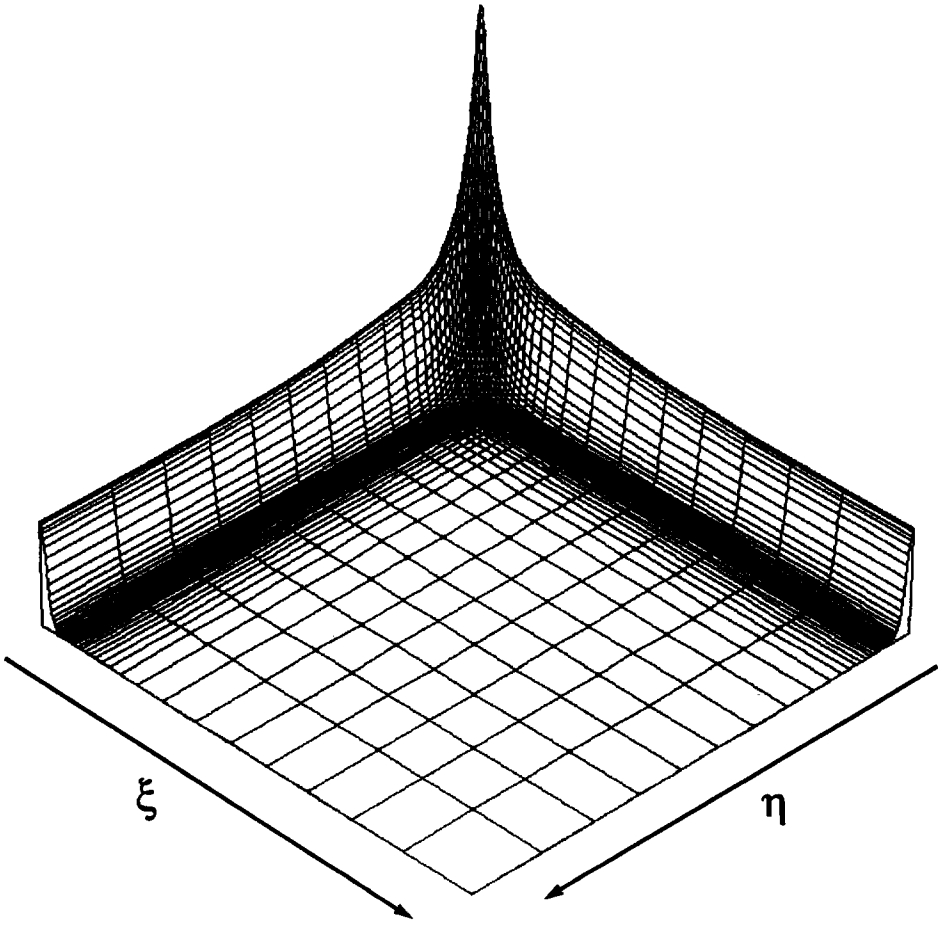

(*a*)

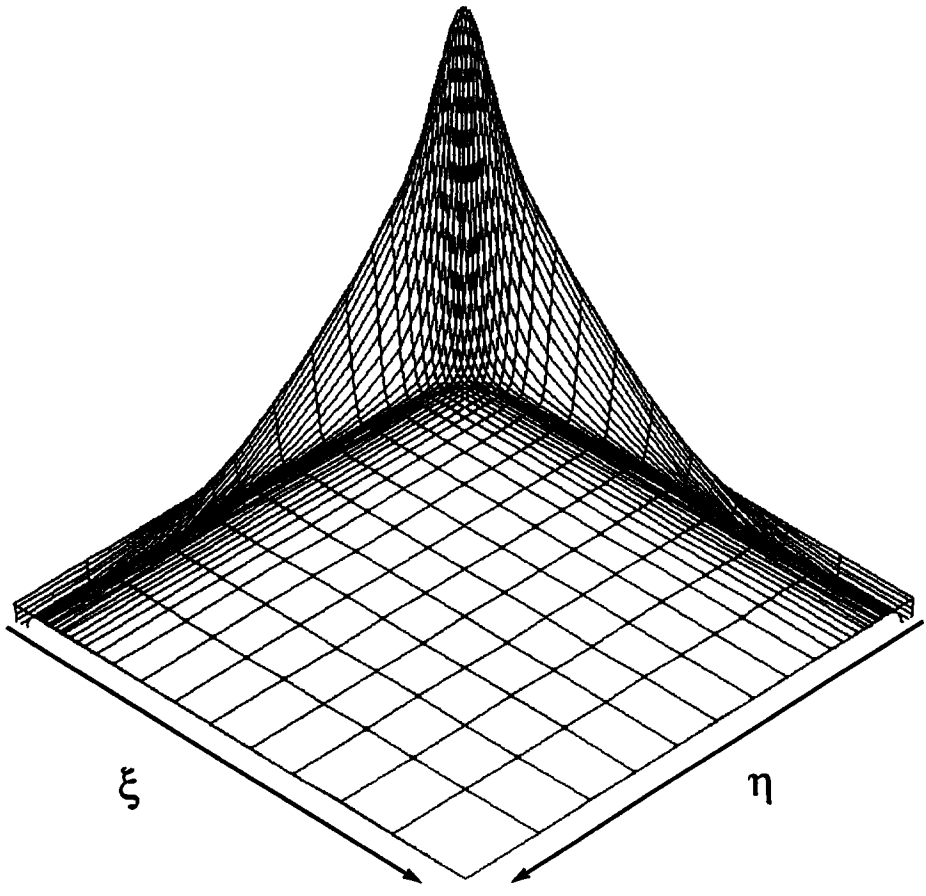

(*b*)

Figure 2(*a*). As in figure 1(*a*) but for $Z=1{\cdot}25$. The vertical scale runs from 0 to 3·25. (*b*). As in figure 1(*b*) but for $Z=1{\cdot}25$. The vertical scale runs from $-2{\cdot}04\times10^{-2}$ to $1{\cdot}85\times10^{-1}$.

5. Discussion

In this paper the range evolution of the full fourth moment of a wavefield propagating from a point source through a random medium has been obtained by numerical solution of the governing partial differential equation. Owing to the wide spread of transverse spatial scales which the fourth moment develops, fixed uniform grid techniques require prohibitively large computational expense. An efficient adaptive grid algorithm has been developed to provide stable and accurate solutions.

The adaptive grid algorithm is not constrained to the relatively modest values of the scattering parameter Γ, used in this paper. Preliminary work with larger values of Γ indicates the possible existence of multiple foci in the scintillation index. Further, in analogy with the results derived for the plane wave [1], it may well turn

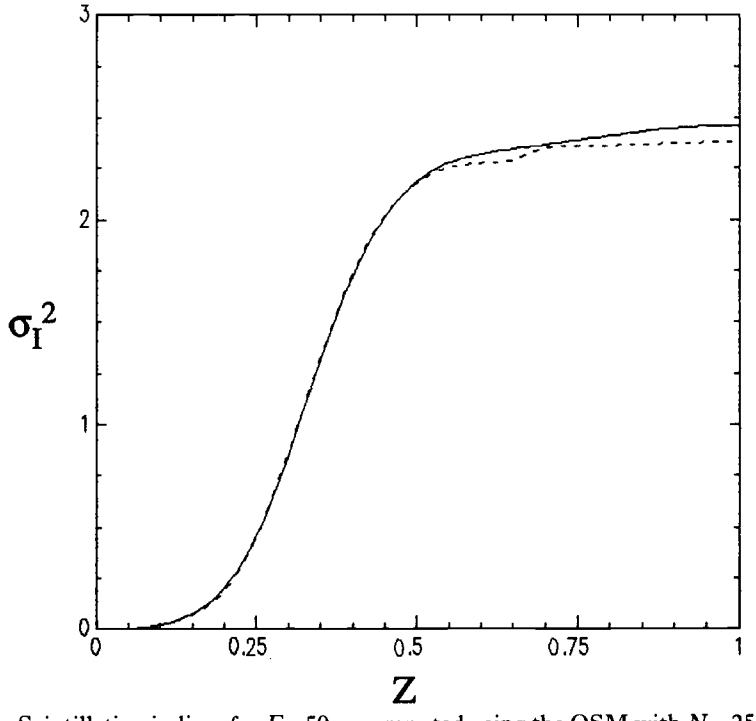

Figure 3. Scintillation indices for $\Gamma = 50$ as computed using the OSM with $N = 256$, broken line, and the AGA with $N = 50$, full line.

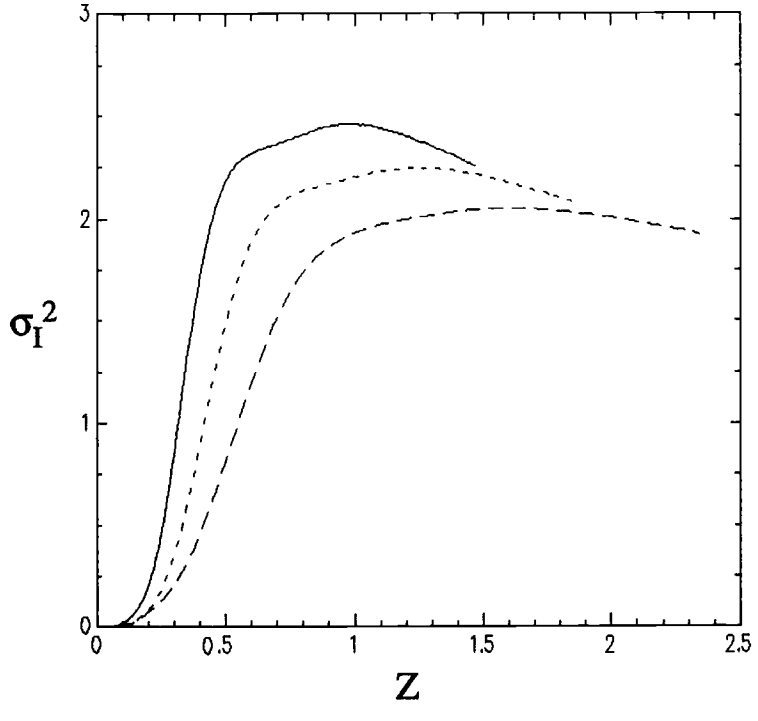

Figure 4. Scintillation indices as functions of range for $\Gamma = 12{\cdot}5$, 25 and 50, dashed, dotted and full lines respectively. All computed with the AGA with $N = 50$ and $H = 2500$.

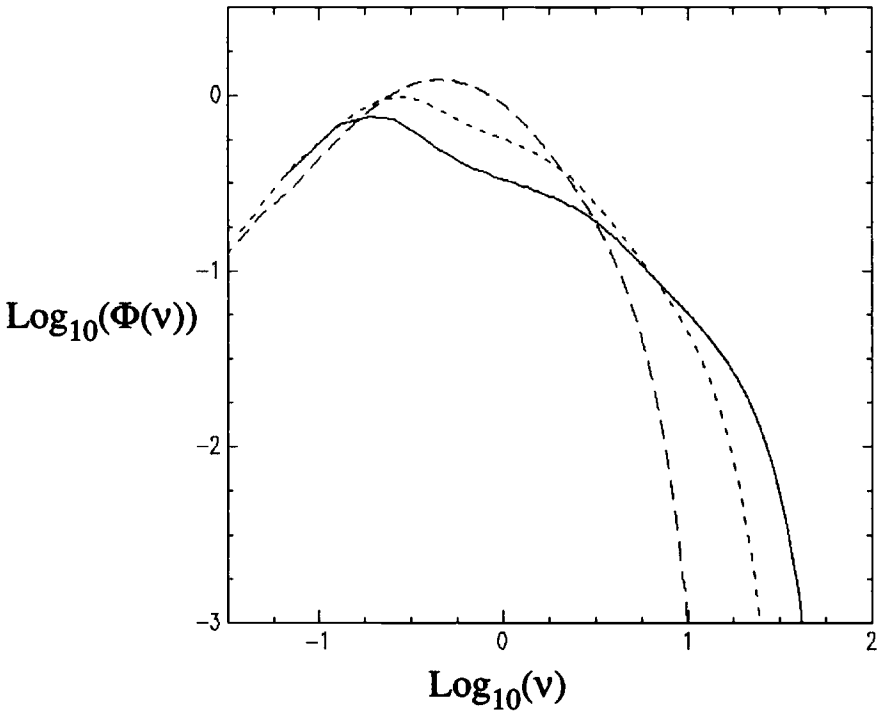

Figure 5. Power spectra for $\Gamma=50$, at $Z=0{\cdot}5$ (dashed), $Z=1{\cdot}0$ (dotted) and $Z=1{\cdot}5$ (full line) respectively.

out that simple laws exist governing the height and position of peaks in the scintillation index for the point source. The structure of the fourth moment suggests that it may be possible to derive analytical approximations for the scintillation index and power spectra using, perhaps, a multi-scale analysis. These topics are currently under investigation and will be addressed in a forthcoming paper.

Acknowledgments

DER and SRL would like to thank Dr A. King for his contributions to the initial stages of the work with the adaptive grid algorithm, and MS is grateful to the Natural Environment Research Council for financial support.

References

[1] Spivack, M., and Uscinski, B. J., 1988, *J. mod. Optics*, **35**, 1741.
[2] Leonard, S. R., Reeve, D. E., and Cook, M. C., 1990, *J. mod. Optics*, **37**, 5.
[3] Uscinski, B. J., 1985, *J. opt. Soc. Am.* A, **2**, 2077.
[4] Macaskill, C., 1983, *Proc. R. Soc. Lond.* A, **386**, 461.
[5] Tur, M., 1985, *J. opt. Soc. Am.* A., **2**, 2161.
[6] Uscinski, B. J., 1989, *J. mod. Optics*, **36**, 1631.
[7] Bhattacharyya, A., and Yeh, K. C., 1988, *Radio Sci.*, **23**, 791.
[8] Sanz-Serna, J. M., and Verwer, J. G., 1985, *IMA J. num. Anal.*, **6**, 25.
[9] Revilla, M. A., 1986, *Int. J. Numer. Methods Engng*, **23**, 2263.
[10] Spivack, M., and Uscinski, B. J., 1989, *J. Comput. appl. Math.*, **27**, 349.